POLYOXOMETALATES

Open Access
MINI REVIEW

# Analytical ultracentrifugation for studying molecular cluster solutions

Ruixin Li[1], Xiaohan Xu[1], Kexing Xiao[1], Bahareh Afsari[1], Lake N. Paul[2], and Tianbo Liu[1] ✉

[1] *School of Polymer Science and Polymer Engineering, The University of Akron, Akron, OH 44325, USA*
[2] *BioAnalysis, LLC, 3401 I Street Suite 206, Philadelphia, PA 19134, USA*

Cite This: *Polyoxometalates*, **2026**, *5*, 9140132

Read Online

**ABSTRACT:** Analytical ultracentrifugation (AUC) is a powerful and information-rich technique for directly characterizing the molecular weight, size, shape, dispersity, and association behavior of species in their native solution environment, spanning a broad molecular weight range of ~ 100 Da to 100 MDa. Unlike many orthogonal methods, AUC does not require immobilization, labeling, or assumptions regarding sample homogeneity. With recent advances in instrumentation and data analysis software, AUC enables more accurate and reliable characterization of diverse solution systems, including biomacromolecules, colloids, surfactants, and polymers. Owing to their uniform and well-defined molecular weights, sizes, and shapes, molecular clusters are particularly well suited for AUC studies. In this work, we investigate molecular cluster solutions using AUC, highlighting its significant potential in this field. Even relatively simple AUC experiments can provide detailed and quantitative insights into molecular cluster systems, including hydration shell thickness, intermolecular distances in dimers, and adsorption of organic ligands such as amino acids.

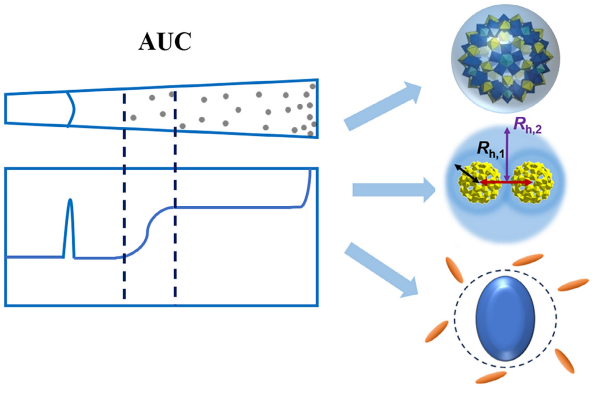


**KEYWORDS:** analytical ultracentrifugation (AUC), molecular clusters, hydration shell thickness, intermolecular distance, surface adsorption

## 1 Introduction

The analytical ultracentrifugation (AUC) technique was developed by Svedberg in the 1920s. He first determined the sizes and size distributions of gold particles below 10 nm [1] using sedimentation velocity AUC (SV-AUC). He subsequently reported the determination of macromolecular molecular weights by sedimentation equilibrium AUC (SE-AUC) in 1925 [2]. These contributions led to the 1926 Nobel Prize in Chemistry "for his work on disperse systems" [3].

Centrifugation operates by applying a strong centrifugal field to a solution containing suspended particles, driving them toward the bottom of the container by sedimentation. The sedimentation rate depends on the applied field strength, solvent viscosity, and the size, shape, and mass of the particles. While conventional centrifugation techniques are widely used in research laboratories, AUC provides an additional capability: It monitors and analyzes individual components in solution during sedimentation. This overcomes a key limitation of techniques such as light and X-ray scattering, which typically measure the collective properties of solute mixtures.

In AUC studies, strong centrifugal fields generated by rotor rotation are applied to dissolved or dispersed samples in AUC cells (Fig. 1(a)). The sedimentation process is monitored using optical detection systems (interference, absorbance, and fluorescence), which measure concentration changes as a function of time and radial position (in SV-AUC), $c(r,t)$, or as a function of radial position at equilibrium (in SE-AUC), $c(r)$. The latest Beckman Coulter Optima AUC model (Fig. 1(b)) operates at rotor speeds of up to 60,000 rpm and can analyze species spanning molecular weights from ~ 100 Da to 100 MDa.

Two principal AUC measurement approaches are used: SV-AUC and SE-AUC. SV-AUC determines sedimentation rates of particles and is primarily applied to assess heterogeneity and size distributions in complex systems. SE-AUC measures the equilibrium distribution of particles in the centrifugal field to determine molar mass and association equilibria. SV-AUC is more commonly used due to its higher throughput and suitability for heterogeneous samples.

The principles of SV-AUC are commonly described by two key equations: the Svedberg equation (Eq. (1)) [1], derived from a force balance during sedimentation without diffusion, and the Lamm equation (Eq. (2)) [5], which describes mass transport arising from both sedimentation and diffusion. The Svedberg equation

**Received:** March 14, 2026; **Revised:** April 17, 2026
**Accepted:** April 21, 2026

✉Address correspondence to tliu@uakron.edu

https://doi.org/10.26599/POM.2026.9140132

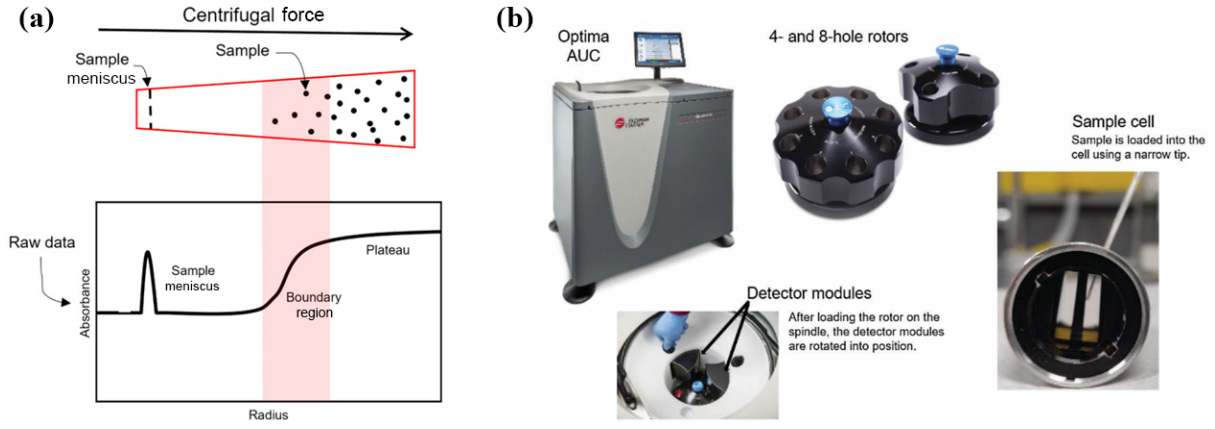


**Figure 1** (a) The illustration of SV-AUC experiment—Sample particles are pushed towards the bottom of the cell by the strong centrifugal force, during the process the particles have been continuously monitored by a UV–Vis detector with time at a fixed location. The absorbance can be inverted to $c(r)$. (b) Hardware of the newest AUC model, Optima AUC, from Beckman Coulter. Images adapted from Beckman Coulter Optima AUC product page (*Beckman Coulter*, accessed February 2, 2026) [4].

establishes a theoretical relationship between the sedimentation coefficient and the molar mass of particles.

$$s \equiv \frac{v}{\omega^2 r} = \frac{M(1-\bar{v}\rho_s)}{f \cdot N_A} \tag{1}$$

Here, $s$ is the sedimentation coefficient (unit: S, 1 S = $10^{-13}$ s), $v$ is the sedimentation velocity, $\omega$ is the angular velocity, $r$ is the radial distance from the axis of rotation, $M$ is the molar mass, $\bar{v}$ is the partial specific volume, $\rho_s$ is the solvent density, $f$ is the frictional coefficient, and $N_A$ is Avogadro's constant. However, in SV-AUC experiments, concentration profiles are not interpreted using this equation directly; instead, $c(r,t)$ data are fitted with numerical solutions of the Lamm equation [6–8], from which both sedimentation and diffusion coefficients are obtained. The Lamm equation describes the time- and radius-dependent evolution of concentration profiles during SV-AUC, explicitly accounting for sedimentation and diffusion. The sedimentation term is represented by $\omega^2 s\left(r\frac{\partial c}{\partial r}+2c\right)$, while the opposing diffusion term arises from concentration gradients ($D\left(\frac{\partial^2 c}{\partial r^2}+\frac{1}{2}\frac{\partial c}{\partial r}\right)$).

$$\frac{\partial c}{\partial t} = D\left(\frac{\partial^2 c}{\partial r^2}+\frac{1}{2}\frac{\partial c}{\partial r}\right) - \omega^2 s\left(r\frac{\partial c}{\partial r}+2c\right) \tag{2}$$

Here, $c$ is the sample concentration, $t$ is time, and $D$ is the diffusion coefficient. In practice, numerical solutions of this equation are fitted to experimental $c(r,t)$ data to extract sedimentation and diffusion coefficients. By combining the Stokes equation (Eq. (3)) with the Svedberg equation (Eq. (1)), the hydrodynamic radius of particles can be obtained:

$$f = 6\pi\eta R_h \tag{3}$$

$$R_h = \frac{M(1-\bar{v}\rho_s)}{6\pi\eta N_A}\omega^2 \tag{4}$$

where $\eta$ is the solvent viscosity and $R_h$ is the hydrodynamic radius of the particles. For spherical particles, the frictional coefficient $f_0$ follows the Stokes relation, where $R_0$ denotes the radius of an equivalent sphere. Therefore, the shape factor $f/f_0$ (also termed the frictional ratio) is defined as follows:

$$f/f_0 = R_h/R_0 \tag{5}$$

For spherical particles, $f/f_0 = 1$, whereas for non-spherical particles, $f/f_0 > 1$. By combining Eqs. (3)–(5), the hydrodynamic radius $R_h$ can be expressed as

$$R_h = \frac{f}{f_0}R_0 = \frac{M(1-\bar{v}\rho_s)}{6\pi\eta N_A s} \tag{6}$$

These relationships enable SV-AUC experiments to provide key particle properties, including sedimentation and diffusion coefficients, size, shape (via the frictional ratio), and molar mass.

Reliable software is essential for analyzing the complex raw data generated by AUC measurements. Advanced tools such as UltraScan III, developed by Borries Demeler [8, 9] and SEDFIT, developed by Peter Schuck [7, 10, 11], are freely available and widely used for AUC data processing.

Multiwavelength AUC (MW-AUC, Fig. 2) can be performed using Beckman Coulter Optima AUC instruments and analyzed with UltraScan. The current system enables data acquisition at up to 20 user-selected wavelengths within the 170–800 nm range through sequential wavelength scanning. However, this instrument does not provide true simultaneous multiwavelength detection. Instead, wavelength selection is achieved using an internal diffraction grating, and measurements at different wavelengths are collected sequentially via grating rotation, resulting in a non-negligible time delay between scans. This delay can be corrected during data analysis, as implemented in UltraScan by Borries Demeler. In contrast, true simultaneous multiwavelength acquisition was first demonstrated by Helmut Cölfen, who developed instrumentation enabling parallel detection across multiple wavelengths [12–15]. These advances allow the analysis of multicomponent solution systems, even when different species have similar sizes and masses, providing they exhibit distinct absorption spectra [16]. The concentration of each species can be determined quantitatively from its specific contribution to the total absorbance, resolved through spectral deconvolution or global fitting of data acquired at multiple wavelengths [17].

AUC offers an inherent advantage in the analysis of multicomponent solutions. When applied to monodisperse systems, it delivers high accuracy and resolution, which underlies its widespread use in the characterization of biomacromolecular solutions with well-defined molecular weights. In contrast, the analysis of synthetic polymers [18, 19] and nanoparticles [12, 19, 20], which are often polydisperse, typically yields lower resolution.

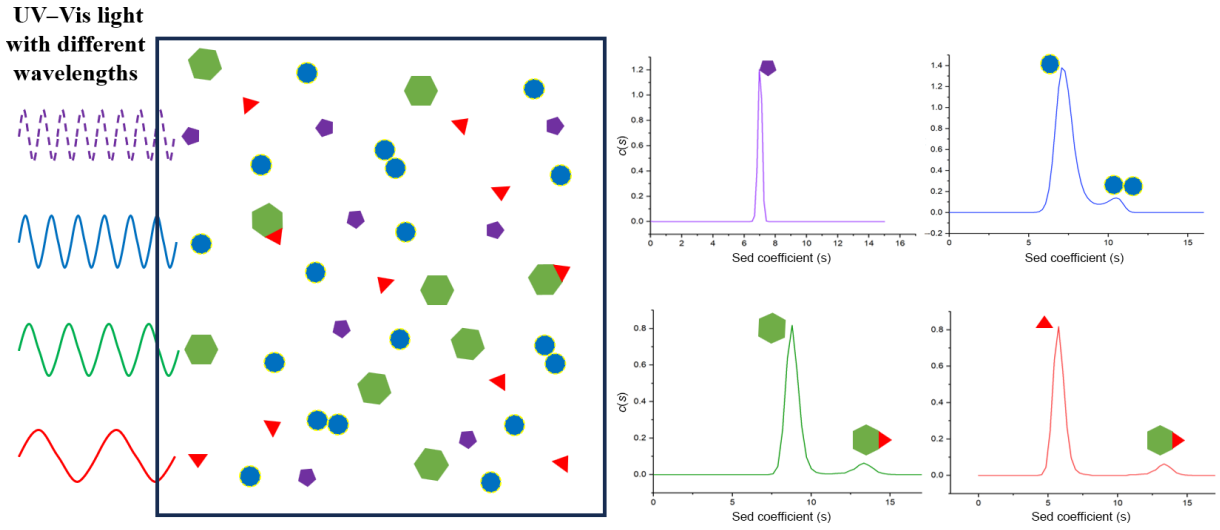


**Figure 2** The illustration of MW-AUC. Species with different colors indicate their different absorbance characteristics. With MW-AUC, this complex solution is resolved by showing that purple particles exist as monomers, blue particles form dimers, green and red particles have a strong binding (the green-red complexes can be detected under both green and red wavelengths). The right part presents the sedimentation coefficient distributions of the particles obtained from multi-wavelength AUC data analysis, where the vertical axis, $c(s)$, represents the concentration.

Over recent decades, AUC has been predominantly applied to biomacromolecules (DNA [21, 22], proteins [23, 24], polysaccharides [25, 26], etc.) supramolecular assemblies, and complex reaction mixtures under native solution conditions. A substantial proportion of these studies has been conducted within the biopharmaceutical sector. Unlike chromatography-based techniques, AUC does not require stationary phases or calibration standards, enabling direct, absolute determination of molar mass from first principles. Because measurements are performed in solution, AUC minimizes artifacts associated with surface interactions and enables the characterization of reversible equilibria without significantly perturbing the system. Its ability to resolve monomers, oligomers, and higher-order aggregates within a single experiment makes it particularly valuable for mechanistic studies, purity assessment, and the evaluation of noncovalent interactions in synthetic and supramolecular organic chemistry.

Owing to their well-defined molecular weights, sizes, and shapes, molecular clusters—particularly polyoxometalate (POM) clusters—are well suited for AUC studies. MW-AUC is especially effective for investigating multicomponent systems and systems involving binding or intermolecular interactions. In the following sections, several representative examples are presented to illustrate the types of information that can be obtained using AUC.

## 2 Determination of hydration shell thickness of molecular clusters

The hydration shell is intrinsically heterogeneous, as the structure and dynamics of water molecules depend on their position relative to the solute surface. In proteins, X-ray and neutron scattering studies show that only water molecules in the first hydration layer exhibit significantly altered structure and dynamics [27]. With increasing distance from the solute, water progressively approaches bulk-like behavior. Complementary techniques, such as nuclear magnetic resonance and THz spectroscopy, further enable characterization of hydration dynamics in nanoparticles. In contrast, AUC does not directly resolve the motion of individual water molecules [28]. Instead, the hydration shell inferred from AUC corresponds to an "effective hydration shell," representing water that is hydrodynamically coupled to the solute and sediments with the clusters.

Recently, the hydration shell thicknesses of a series of metal–oxide and metal–peroxide molecular clusters, including Keggins, Keplerates, $\{P_2W_{17}\}$, and uranium peroxide nanocages, were determined using SV-AUC [29]. From the measured sedimentation coefficients, $R_h$ of these clusters can be calculated with angstrom-level resolution using Eq. (6). The hydration shell thickness is then obtained by subtracting the radius of the bare cluster from $R_h$ (Fig. 3(a)). For monodisperse cluster solutions, SV-AUC yields sedimentation coefficients with low residuals and narrow distributions (Figs. 3(b) and 3(c)), enabling precise estimation of $R_h$. Clusters with very high charge density (e.g., $\{U_{60}\}$ and $\{U_{24}Pp_{12}\}$) exhibit co-sedimentation of approximately three layers of water molecules (assuming $R_h$ of ~ 0.14 nm per water molecule). In contrast, the weakly charged cluster $\{Mo_{72}Fe_{30}\}$ (−7 in aqueous solution) carries only a single water layer. Two notable exceptions are the Keggin clusters $\{PW_{12}\}$ and $\{SiW_{12}\}$, which exhibit little to no effective hydration layer; only a small number of weakly associated water molecules co-sediment with the clusters rather than forming a continuous shell. This unusually thin hydration shell is consistent with early observations by John F. Pope in 1960 [30] and with their superchaotropic character, reflecting a strong affinity for neutral domains in aqueous environments.

Three factors influencing hydration shell thickness were examined: surface charge density, solution pH, and temperature. SV-AUC measurements show an approximately linear increase in hydration shell thickness with increasing surface charge density (Fig. 4(a)). In addition, $\{Mo_{72}Fe_{30}\}$ behaves as a weak acid; higher pH promotes deprotonation, increasing its effective charge and resulting in a thicker hydration shell, as observed by AUC (Fig. 4(b)). The hydration shell of $\{Mo_{72}Fe_{30}\}$ is very thin (~ 0.05 nm) at pH = 2.26, indicating minimal associated water, but increases to ~ 0.21 nm at pH = 4.45. This trend supports the conclusion that hydration shell thickness in these rigid clusters is primarily governed by surface charge density. In contrast,

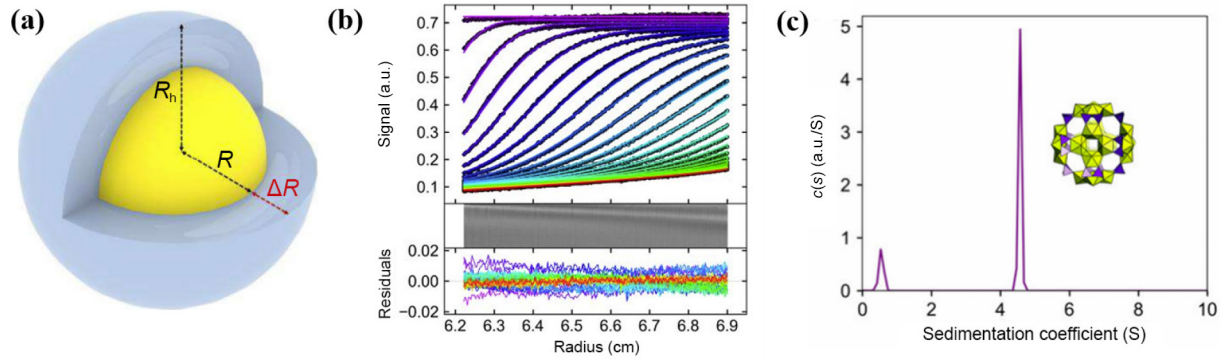


**Figure 3** (a) Core–shell model of a hydrated molecular cluster, where $R$ is the bare radius of the cluster, $R_h$ is the hydrodynamic radius of the hydrated molecule, and $\Delta R$ is the thickness of the hydration shell. The SV analysis (from SEDFIT) of the $\{U_{24}Pp_{12}\}$ solution. (b) The fits of raw data (upper panel) and residual plots (lower panel), where AU is the absorbance unit, and the radius refers to the distance from the center of rotation to a given point in the solution. (c) The sedimentation coefficient distribution. Adapted with permission from Ref. [29], © American Chemical Society 2025.

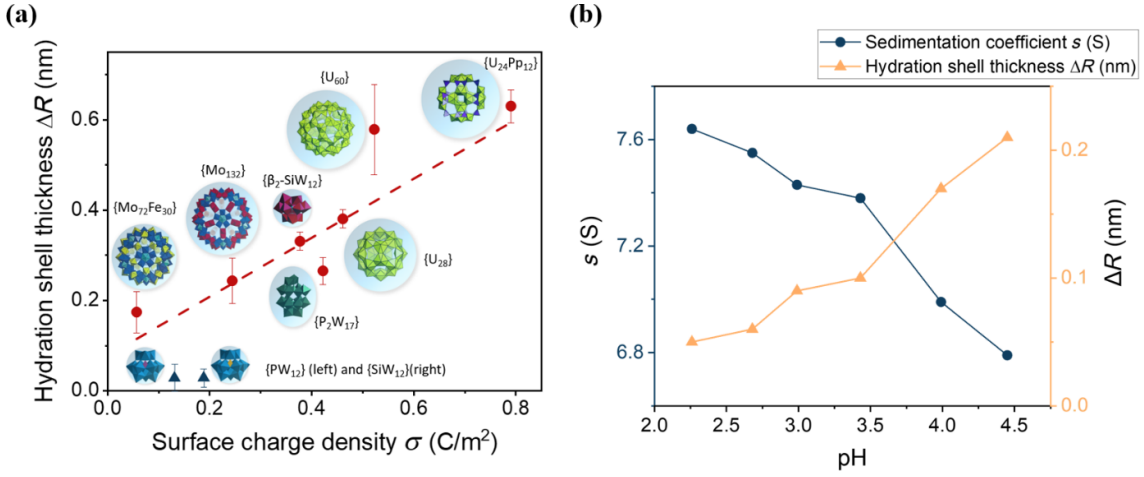


**Figure 4** (a) Dependence of hydration shell thickness of molecular clusters in aqueous solutions on surface charge density. The hydration shell thickness is found to increase with increasing charge density on the clusters, from about one layer of water for $\{Mo_{72}Fe_{30}\}$ to about three layers for $\{U_{24}Pp_{12}\}$. The exceptions are some Keggins which carry negligible amounts of hydrated water molecules. (b) Dependence of sedimentation coefficient and hydration shell thickness of $\{Mo_{72}Fe_{30}\}$ cluster in aqueous solution on pH. Adapted with permission from Ref. [29], © American Chemical Society 2025.

temperature has a much weaker effect. SV-AUC measurements of highly charged $\{U_{24}Pp_{12}\}$ macroions at different temperatures show only a slight decrease in hydration shell thickness at elevated temperatures. This behavior is consistent with hydration dominated by electrostatic interactions, which are relatively insensitive to temperature over the range studied.

## 3 Determination of intermolecular distance of dimers in molecular cluster solutions

The size disparity between nanoscale macroions (e.g., POMs) and their small counterions leads to relatively loose macroion–counterion association, particularly for heavy, multivalent counterions [31]. This weak association is qualitatively reflected in AUC measurements, where sedimentation behavior shifts with increasing apparent molar mass and hydrodynamic radius. However, anomalous small-angle X-ray scattering (ASAXS) can provide more precise determination of the number of associated counterions and their spatial distribution around the cluster, providing the counterions are suitable elements such as $Rb^+$ or $Sr^{2+}$ [32]. When counterion association becomes sufficiently strong, counterion-mediated attraction between like-charged macroions can occur. This interaction is a key factor governing the solution behavior and phase transitions of charged POM systems. For example, the $\{U_{60}\}$ cluster ($Li_{48}K_{12}[UO_2(O_2)(OH)]_{60}{\cdot}211H_2O$) [33] exhibits counterion-dependent solution and microphase transitions. A series of phase behaviors of $\{U_{60}\}$ has been systematically investigated, including the formation of single-layered, hollow, spherical "blackberry" assemblies in solution, as well as gelation and phase–phase separation (coacervation) [34, 35]. $\{U_{60}\}$ dimers represent the initial stage of macroion self-assembly. These species can further associate into oligomers and subsequently into flexible two-dimensional (2D) nanosheets, which tend to bend and close to form hollow, spherical "blackberry" structures that are thermodynamically stable in dilute solution. In the presence of strongly binding counterions, the formation of more rigid 2D sheets can also induce macrophase transitions from solution to gel or coacervate. Therefore, determining the intermolecular distance between $\{U_{60}\}$ units in the dimer state is essential for understanding its phase behavior.

Recently, we reported the determination of the intermolecular distance of $\{U_{60}\}$ dimers in their self-assembled states across coacervate, gel, and solution phases, respectively [36]. The intermolecular distance in the $\{U_{60}\}$ dimer was obtained using SV-AUC. In particular, the hydrodynamic radii of the monomer ($R_{h,1}$) and dimer ($R_{h,2}$) were derived from their corresponding

sedimentation coefficients ($s_1$ and $s_2$) using Eq. (6) and the relation $s_2/s_1 = 2R_{h,1}/R_{h,2}$. Because dimers are non-spherical, dedicated hydrodynamic modeling software such as HYDRO++ [37] is required to convert the equivalent-sphere $R_{h,2}$ into a physically meaningful geometry, enabling determination of the intermolecular distance between two {$U_{60}$} units (Fig. 5). As shown in Fig. 5, the $R_h$ of the {$U_{60}$} monomer and dimer in a $Y^{3+}$–{$U_{60}$} (molar ratio = 5) solution are approximately 1.63 and 2.09 nm, respectively. The inter-{$U_{60}$} distance was determined to be ~ 2.88 nm from HYDRO++ fitting.

In SV-AUC experiments, a pure aqueous {$U_{60}$} solution and a series of {$U_{60}$} solutions containing different counterions ($Rb^+$, $K^+$, and $Y^{3+}$) were characterized (Fig. 6). Compared with the radius of the bare {$U_{60}$} cluster in the crystalline state (~1.21 nm) [28], the $R_h$ of {$U_{60}$} in solution (based on $s$ = 7.58 S) is larger (~ 1.79 nm), reflecting the contribution of the hydration shell. As shown in Fig. 6, monomeric {$U_{60}$} exhibits an increased $s$ upon addition of heavier counterions, corresponding to a decrease in $R_{h,1}$. This trend can be attributed to partial disruption of the hydration shell and increased counterion association around the {$U_{60}$} clusters. Due to counterion association, each {$U_{60}$} cluster carries fewer charges, leading to a reduced hydration shell thickness and a smaller $R_h$. Moreover, the $s$ ratio ($s_2/s_1$) of the {$U_{60}$} dimer reflects the intermolecular separation, with a larger $s$ ratio indicating a shorter {$U_{60}$}–{$U_{60}$} distance in solution. In addition, the trend in inter-{$U_{60}$} distance reflects the relative strength of counterion interactions, following the order: {$U_{60}$}–$Y^{3+}$ > {$U_{60}$}–$K^+$ > {$U_{60}$}–$Rb^+$. This hierarchy is consistent with the observed solution behavior of {$U_{60}$} macroions. The addition of $Y^{3+}$ promotes the formation of rigid 2D nanosheets, whereas $K^+$ favors blackberry-type assemblies, and $Rb^+$ leads to smaller blackberry structures. Weaker counterion-mediated attraction allows the resulting 2D sheets to bend more readily, facilitating curvature-driven assembly.

Combining SAXS measurements of inter-{$U_{60}$} distances in the gel state leads to the conclusion that the intermolecular distance of {$U_{60}$} increases progressively during phase transitions (Fig. 7). Counterion-mediated attraction between {$U_{60}$} macroions establishes a characteristic {$U_{60}$}–{$U_{60}$} separation in solution, which increases as the strength or valence of the counterions decreases. The intermolecular distance increases from ~ 2.68 nm in {$U_{60}$} single crystals to ~ 2.74 nm at higher {$U_{60}$} concentrations in the presence of $Y^{3+}$ ions. It further increases to ~ 2.88 nm in the dimeric state at lower {$U_{60}$} concentrations with reduced $Y^{3+}$ content, then to ~ 3.09 nm in the presence of weaker $K^+$ counterions, and finally to ~ 3.26 nm for dimers with the addition of even weaker $Rb^+$ ions. This systematic increase in intermolecular distance correlates well with the self-assembly behavior and macrophase transitions of {$U_{60}$} in aqueous solutions.

## 4 Adsorption of amino acids onto molecular cluster surfaces

In aqueous solution, molecular clusters can interact with a variety of species through noncovalent interactions, including hydrogen bonding [38, 39], electrostatic interactions [40, 41], and host–guest interactions [42, 43]. As the fundamental building blocks of proteins, amino acids serve as simplified yet chemically relevant model systems for probing interactions between molecular clusters and biomolecules, while retaining key functional groups and chirality. Notably, their adsorption onto inorganic surfaces is

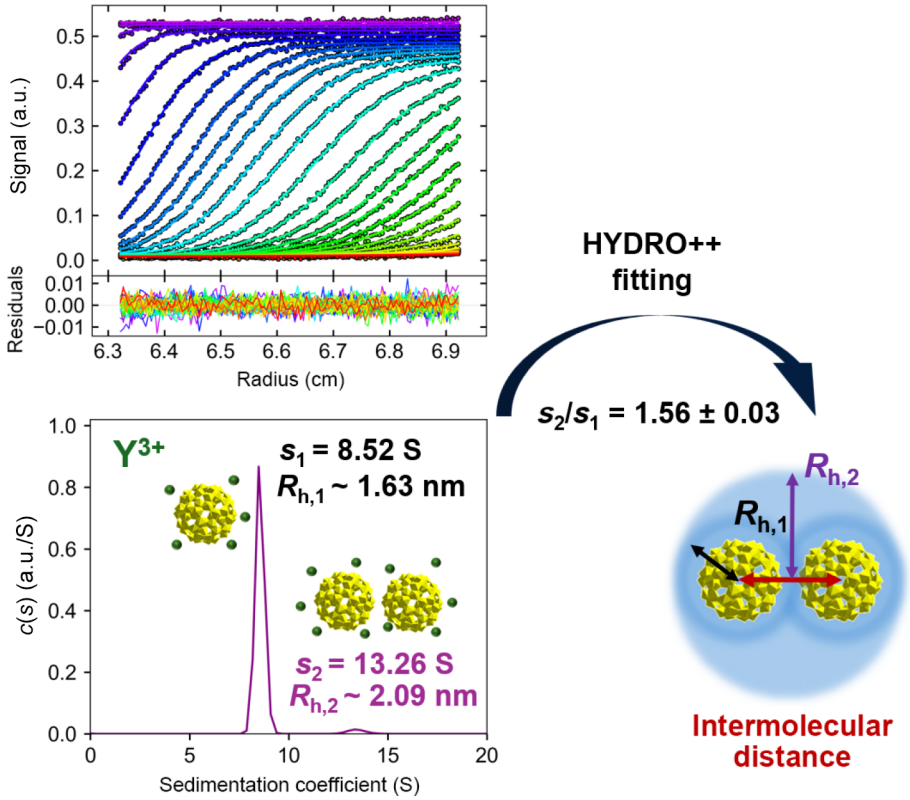


**Figure 5** Measurement of intermolecular distance of {$U_{60}$} macroions dimer in solutions by SV-AUC. SV-AUC analysis from SEDFIT (left two figures) provides the sedimentation coefficient of {$U_{60}$} monomer and dimer in solutions. From the ratio between the $R_h$ values of monomers and dimers, the intermolecular distance between the dimers can be calculated. Adapted with permission from Ref. [36], © American Chemical Society 2025.

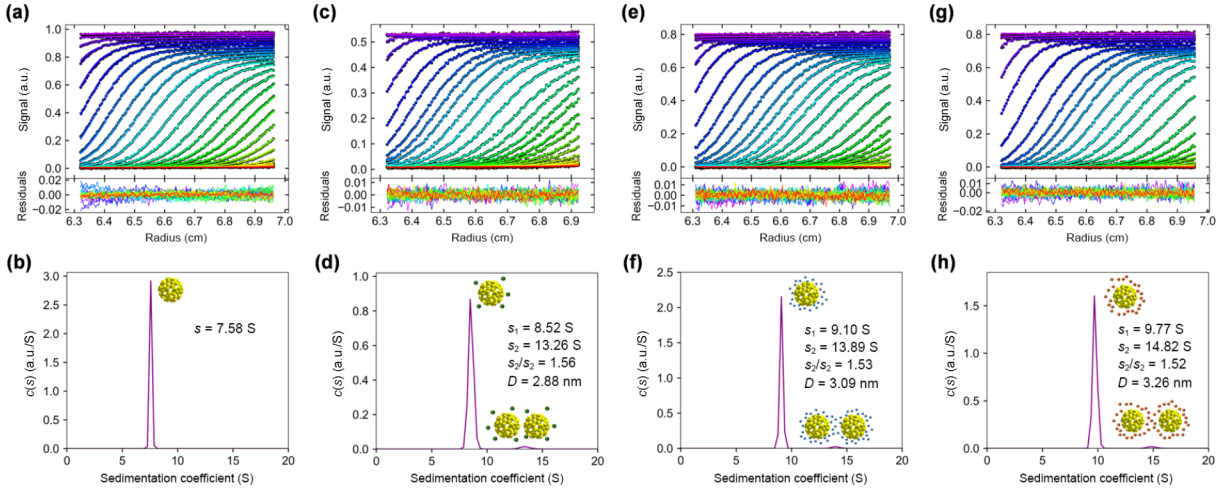


**Figure 6** SV analysis (from SEDFIT) of $\{U_{60}\}$ dilute sample solutions, where $s_1$ is the sedimentation coefficient of $\{U_{60}\}$ monomer, $s_2$ is the sedimentation coefficient of $\{U_{60}\}$ dimer, $D$ is the inter-$\{U_{60}\}$ distance. SV experiments of (a) pure $\{U_{60}\}$ aqueous solution, (c) $\{U_{60}\}$-$Y^{3+}$ (molar ratio = 5) aqueous solution, (e) $\{U_{60}\}$-$K^+$ (molar ratio = 48) aqueous solution and (g) $\{U_{60}\}$-$Rb^+$ (molar ratio = 48) aqueous solution run at 40,000 rpm and 20 °C fitted by $c(s)$ model. (b), (d), (f) and (h) are the sedimentation coefficient distributions of (a), (c), (e) and (g), respectively. $\{U_{60}\}$ dimers are observed in (d), (f) and (h), upon addition of $Y^{3+}$ counterions (small green spheres), $K^+$ counterions (small blue spheres) and $Rb^+$ counterions (small orange spheres), respectively. Adapted with permission from Ref. [36], © American Chemical Society 2025.

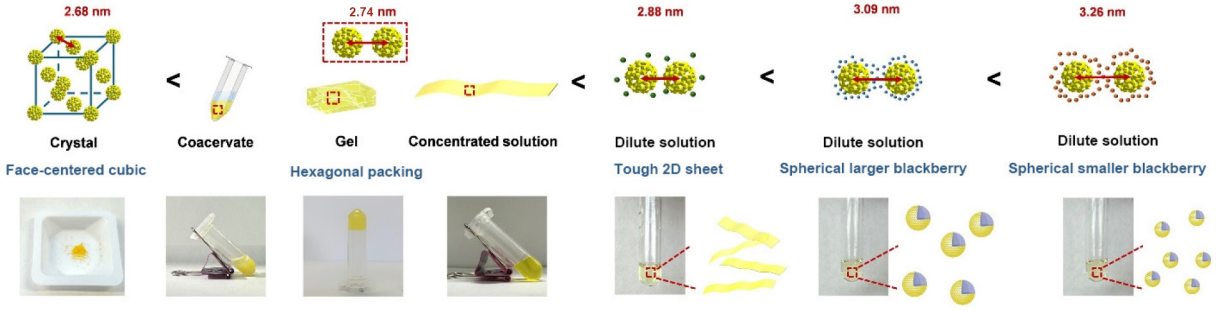


**Figure 7** Intermolecular distance of $\{U_{60}\}$ macroions in different phase status. From single crystals (with van der Waals distance, the nearest possible inter-cluster distance) to coacervates (liquid–liquid phase separation), gels (homogeneous phase) to solutions containing standalone 2D sheets, large blackberry structures and smaller blackberry structures, the inter-$\{U_{60}\}$ distance gradually increases. Reprinted with permission from Ref. [36], © American Chemical Society 2025.

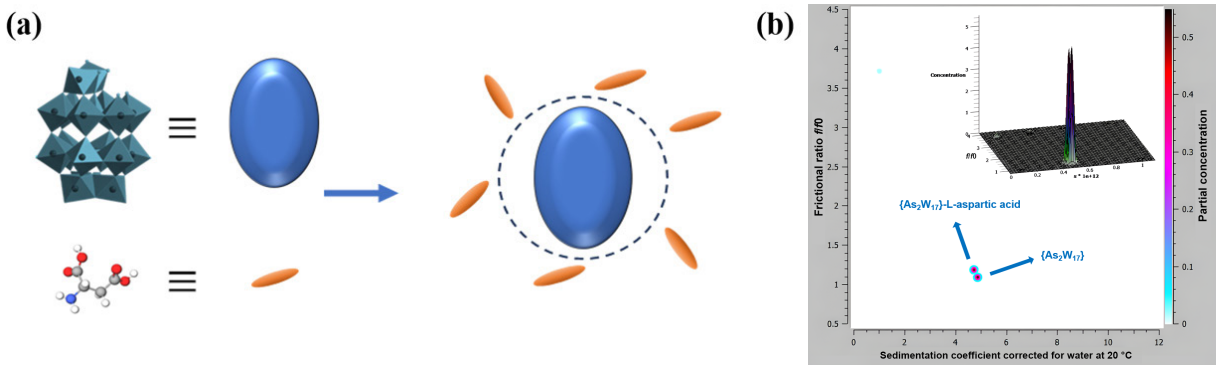


**Figure 8** (a) The simplified structures of $\{As_2W_{17}\}$ and alanine, along with the proposed adsorption mechanism of Aspartic acid onto $\{As_2W_{17}\}$. The dashed line indicates the hydrodynamic radius of the $\{As_2W_{17}\}$ cluster. (b) The sedimentation coefficient distribution (from UltraScan III) of $\{As_2W_{17}\}$ solution with L-aspartic acid. Two species were observed by AUC: individual $\{As_2W_{17}\}$ clusters and the binding product of L-aspartic acid onto $\{As_2W_{17}\}$.

governed by extremely subtle interfacial forces that are often below the detection limits of conventional techniques but can be sensitively resolved using AUC. Figure 8 presents SV-AUC results for the adsorption of amino acids onto $\{As_2W_{17}\}$ ($K_{10}[As_2W_{17}O_{61}]\cdot 15H_2O$) [44]. Two species in solution—free $\{As_2W_{17}\}$ and the $\{As_2W_{17}\}$–aspartic acid complex—can be clearly distinguished by AUC. SV-AUC analysis using UltraScan III provides access to key parameters, including molecular weight, sedimentation and diffusion coefficients, frictional ratio ($f/f_0$), and species concentration, as well as the number of species present and their relative populations in solution. By combining the experimentally determined molecular weight with the known mass of aspartic acid, the number of adsorbed amino acids per inorganic cluster can be directly quantified. In addition, a slight conformational or shape change upon adsorption is indicated by an increase in $f/f_0$ to ~ 1.2.

## 5 Conclusions

AUC is a powerful technique for investigating complex solution systems. Owing to their well-defined and uniform size, shape, and mass, molecular clusters are particularly well suited for AUC measurements. The examples presented in this study demonstrate the effectiveness of AUC in determining hydration shell thicknesses of clusters, intermolecular distances in dimers, and the association between molecular clusters and amino acid ligands. Additional applications of AUC include the detection of cluster dissociation, oligomer formation, selective binding between clusters and other species, and host–guest interactions involving cage-like molecules. Although large supramolecular assemblies of clusters are not discussed in detail in this study, such systems are also amenable to AUC analysis due to its high sensitivity. For example, AUC can be used to accurately determine the mass of self-assembled blackberry structures in aqueous solution. While some of these properties can be probed using alternative techniques, AUC offers the distinct advantage of resolving different species prior to analysis, enabling direct determination of their individual concentrations. This capability is critical for accurate molar mass determination.

Moreover, MW-AUC is a powerful technique for studying cluster-containing solutions. Many such systems comprise multiple components, and differences in their absorption spectra enable MW-AUC to resolve individual species. This makes it particularly useful for investigating competitive cluster–ligand binding and host–guest interactions involving cage-like molecules. However, the technique requires substantial expertise, experience, and instrumentation resources. As a result, the barrier to entry for new users can be relatively high, with a need for extensive training covering both experimental operation and data analysis.

## Data availability

All data needed to support the conclusions in the paper are presented in the manuscript. Additional data related to this paper may be requested from the corresponding author upon request.

## Acknowledgments

T. B. L. acknowledges support from the University of Akron.

## Declaration of competing interest

All the contributing authors report no conflict of interests in this work. Author Tianbo Liu is one of the Associate Editors of this journal, but he is not involved in the peer-review or decision of this article.

## Author contribution statement

R. X. L.: Data curation, visualization, writing – original draft, writing – review & editing. X. H. X., K. X. X, B. A., and L. N. P.: Writing – review & editing. T. B. L: Funding support, supervision, writing – review & editing. All the authors have approved the final manuscript.

## Use of AI statement

None.

## References

[1] Svedberg, T.; Nichols, J. B. Determination of size and distribution of size of particle by centrifugal methods. *J. Am. Chem. Soc.* **1923**, *45*, 2910–2917.

[2] Svedberg, T.; Fåhraeus, R. A new method for the determination of the molecular weight of proteins. *J. Am. Chem. Soc.* **1926**, *48*, 430–438.

[3] Svedberg, T. *The Nobel Prize in Chemistry 1926-Summary* [Online]. https://www.nobelprize.org/prizes/chemistry/1926/summary/(accessed Feb 2, 2026).

[4] Optima Analytical Ultracentrifuges. *Beckman Coulter* [Online]. https://www.beckman.com/centrifuges/analytical-ultracentrifuges/optima-auc (accessed Feb 2, 2026).

[5] Lamm, O. *Die Differentialgleichung der Ultrazentrifugierung*; Almqvist & Wiksell, 1929.

[6] Schuck, P.; Demeler, B. Direct sedimentation analysis of interference optical data in analytical ultracentrifugation. *Biophys. J.* **1999**, *76*, 2288–2296.

[7] Schuck, P.; Rossmanith, P. Determination of the sedimentation coefficient distribution by least-squares boundary modeling. *Biopolymers* **2000**, *54*, 328–341.

[8] Brookes, E.; Cao, W. M.; Demeler, B. A two-dimensional spectrum analysis for sedimentation velocity experiments of mixtures with heterogeneity in molecular weight and shape. *Eur. Biophys. J.* **2010**, *39*, 405–414.

[9] Demeler, B.; Gorbet, G. E. Analytical ultracentrifugation data analysis with UltraScan-III. In *Analytical Ultracentrifugation: Instrumentation, Software, and Applications*; Uchiyama, S.; Arisaka, F.; Stafford, W. F.; Laue, T., Eds.; Springer: Tokyo, 2016; pp 119–143.

[10] Schuck, P. Size-distribution analysis of macromolecules by sedimentation velocity ultracentrifugation and lamm equation modeling. *Biophys. J.* **2000**, *78*, 1606–1619.

[11] Schuck, P. *Sedimentation Velocity Analytical Ultracentrifugation: Discrete Species and Size-Distributions of Macromolecules and Particles*; CRC Press: Boca Raton, 2016.

[12] Cölfen, H. Analytical ultracentrifugation in colloid and polymer science: New possibilities and perspectives after 100 years. *Colloid Polym. Sci.* **2023**, *301*, 821–849.

[13] Pearson, J. Z.; Krause, F.; Haffke, D.; Demeler, B.; Schilling, K.; Cölfen, H. Next-generation AUC adds a spectral dimension: Development of multiwavelength detectors for the analytical ultracentrifuge. *Methods Enzymol.* **2015**, *562*, 1–26.

[14] Bhattacharyya, S. K.; Maciejewska, P.; Börger, L.; Stadler, M.; Gülsün, A. M.; Cicek, H. B.; Cölfen, H. Development of a fast fiber based UV-Vis multiwavelength detector for an ultracentrifuge. In *Proceedings of the Analytical Ultracentrifugation VIII*, Berlin, Germany, 2006, pp 9–22.

[15] Strauss, H. M.; Karabudak, E.; Bhattacharyya, S.; Kretzschmar, A.; Wohlleben, W.; Cölfen, H. Performance of a fast fiber based UV/Vis multiwavelength detector for the analytical ultracentrifuge. *Colloid Polym. Sci.* **2008**, *286*, 121–128.

[16] Mortezazadeh, S.; Demeler, B. A spectral decomposition quality assessment tool for multi-wavelength AUC experiments with UltraScan. *Eur. Biophys. J.* **2023**, *52*, 303–310.

[17] Demeler, B. Measuring molecular interactions in solution using multi-wavelength analytical ultracentrifugation: Combining spectral analysis with hydrodynamics. *Biochemist* **2019**, *41*, 14–18.

[18] Diaz, L.; Peyrot, C.; Wilkinson, K. J. Characterization of polymeric nanomaterials using analytical ultracentrifugation. *Environ. Sci. Technol.* **2015**, *49*, 7302–7309.

[19] Cölfen, H. Analytical ultracentrifugation of colloids. In *Analytical Ultracentrifugation: Techniques and Methods*; Scott, D. J., Harding, S. E., Rowe, A. J., Eds.; Royal Society of Chemistry: Cambridge, UK, **2005**; pp 501–583.

[20] Planken, K. L.; Cölfen, H. Analytical ultracentrifugation of colloids.

*Nanoscale* **2010**, *2*, 1849–1869.
[21] Tennyson, R. B.; Lindsley, J. E. Type II DNA topoisomerase from *Saccharomyces cerevisiae* is a stable dimer. *Biochemistry* **1997**, *36*, 6107–6114.
[22] Yang, T. C.; Catalano, C. E.; Maluf, N. K. Analytical ultracentrifugation as a tool to study nonspecific protein-DNA interactions. *Methods Enzymol.* **2015**, *562*, 305–330.
[23] Lebowitz, J.; Lewis, M. S.; Schuck, P. Modern analytical ultracentrifugation in protein science: A tutorial review. *Protein Sci.* **2002**, *11*, 2067–2079.
[24] Howlett, G. J.; Minton, A. P.; Rivas, G. Analytical ultracentrifugation for the study of protein association and assembly. *Curr. Opin. Chem. Biol.* **2006**, *10*, 430–436.
[25] Harding, S. E. Challenges for the modern analytical ultracentrifuge analysis of polysaccharides. *Carbohydr. Res.* **2005**, *340*, 811–826.
[26] Harding, S. E. Analysis of polysaccharides by ultracentrifugation. Size, conformation and interactions in solution. In *Polysaccharides I: Structure, Characterization and Use*; Heinze, T., Ed.; Springer: Berlin Heidelberg, 2005; pp 211–254.
[27] Halle, B. Protein hydration dynamics in solution: A critical survey. *Philos. Trans. R. Soc. Lond B: Biol. Sci.* **2004**, *359*, 1207–1224.
[28] Zobel, M. Observing structural reorientations at solvent-nanoparticle interfaces by X-ray diffraction-putting water in the spotlight. *Acta Crystallogr. Sect. A: Found. Adv.* **2016**, *72*, 621–631.
[29] Xu, X. H.; Li, R. X.; Xiao, K. X.; Afsari, B.; Zhou, Y. F.; Szymanowski, J. E. S.; Sundar, A.; Burns, P. C.; Kortz, U.; Liu, T. B. Direct determination of hydration shell thickness of molecular clusters. *Inorg. Chem.* **2026**, *65*, 101–108.
[30] Baker, L. C. W.; Pope, M. T. The identical diffusion coefficients of isostructural heteropoly anions. The complete independence of D from ionic weight. *J. Am. Chem. Soc.* **1960**, *82*, 4176–4179.
[31] Liu, T. B. Hydrophilic macroionic solutions: What happens when soluble ions reach the size of nanometer scale? *Langmuir* **2010**, *26*, 9202–9213.
[32] Chen, J. H.; Bera, M. K.; Li, H.; Yang, Y. Q.; Sun, X. Y.; Luo, J. C.; Baughman, J.; Liu, C.; Yao, X. S.; Chuang, S. S. C. et al. Accurate determination of the quantity and spatial distribution of counterions around a spherical macroion. *Angew. Chem., Int. Ed.* **2021**, *60*, 5833–5837.
[33] Sigmon, G. E.; Unruh, D. K.; Ling, J.; Weaver, B.; Ward, M.; Pressprich, L.; Simonetti, A.; Burns, P. C. Symmetry versus minimal pentagonal adjacencies in uranium-based polyoxometalate fullerene topologies. *Angew. Chem., Int. Ed.* **2009**, *48*, 2737–2740.
[34] Xiao, K. X.; Yang, Y. Q.; Xu, X. H.; Szymanowski, J. E. S.; Zhou, Y. F.; Sigmon, G. E.; Burns, P. C.; Liu, T. B. Coacervate formation in dilute aqueous solutions of inorganic molecular clusters with simple divalent countercations. *Inorg. Chem.* **2024**, *63*, 15331–15339.
[35] Xu, X. H.; Yang, Y. Q.; Zhou, Y. F.; Xiao, K. X.; Szymanowski, J. E. S.; Sigmon, G. E.; Burns, P. C.; Liu, T. B. Critical conditions regulating the gelation in macroionic cluster solutions. *Adv. Sci.* **2024**, *11*, 2308902.
[36] Xiao, K. X.; Zhou, Y. F.; Szymanowski, J. E. S.; Xu, X. H.; Chodankar, S.; Burns, P. C.; Liu, T. B. Determination of intermolecular distances in dilute solutions of macroions and their direct correlations with self-assembly and macrophase transitions. *J. Am. Chem. Soc.* **2025**, *147*, 24913–24920.
[37] García de la Torre, J.; del Rio Echenique, G.; Ortega, A. Improved calculation of rotational diffusion and intrinsic viscosity of bead models for macromolecules and nanoparticles. *J. Phys. Chem. B* **2007**, *111*, 955–961.
[38] Zhou, J.; Hu, J.; Li, M.; Li, H.; Wang, W. Y.; Liu, Y. Z.; Winans, R. E.; Li, T.; Liu, T. B.; Yin, P. C. Hydrogen bonding directed co-assembly of polyoxometalates and polymers to core-shell nanoparticles. *Mater. Chem. Front.* **2018**, *2*, 2070–2075.
[39] Liu, Q. D.; Yu, H. D.; Zhang, Q. H.; Wang, D.; Wang, X. Temperature-responsive self-assembly of single polyoxometalates clusters driven by hydrogen bonds. *Adv. Funct. Mater.* **2021**, *31*, 2103561.
[40] Kobayashi, D.; Nakahara, H.; Shibata, O.; Unoura, K.; Nabika, H. Interplay of hydrophobic and electrostatic interactions between polyoxometalates and lipid molecules. *J. Phys. Chem. C* **2017**, *121*, 12895–12902.
[41] Arefian, M.; Mirzaei, M.; Eshtiagh-Hosseini, H.; Frontera, A. A survey of the different roles of polyoxometalates in their interaction with amino acids, peptides and proteins. *Dalton Trans.* **2017**, *46*, 6812–6829.
[42] Wu, Y. L.; Shi, R. F.; Wu, Y. L.; Holcroft, J. M.; Liu, Z. C.; Frasconi, M.; Wasielewski, M. R.; Li, H.; Stoddart, J. F. Complexation of polyoxometalates with cyclodextrins. *J. Am. Chem. Soc.* **2015**, *137*, 4111–4118.
[43] Yu, R. M.; Kuang, X. F.; Wu, X. Y.; Lu, C. Z.; Donahue, J. P. Stabilization and immobilization of polyoxometalates in porous coordination polymers through host-guest interactions. *Coord. Chem. Rev.* **2009**, *253*, 2872–2890.
[44] Contant, R.; Klemperer, W. G.; Yaghi, O. Potassium octadecatungstodiphosphates(V) and related lacunary compounds. In *Inorganic Syntheses*; Ginsberg, A. P., Ed.; Inorganic Syntheses, Inc., 1990; pp 104–111.

**Ruixin Li** received his B.S. in School of Emergent Soft Matter from South China University of Technology (SCUT) in 2023. Then he received his M.S. degree in 2024 at University of Akron in School of Polymer Science and Polymer Engineering under the supervision of Professor Tianbo Liu. He is currently in the same group as a PhD student. His current research interests focus on solution behaviors of macroion.

**Xiaohan Xu** received her Bachelor's degree from Qingdao University of Science and Technology and her Master's degree from the University of Akron. She is currently pursuing a Ph.D. in Polymer Science under the supervision of Prof. Tianbo Liu. Her research focuses on the phase behavior of molecular cluster solutions and the self-assembly of inorganic–organic hybrid amphiphiles.

**Kexing Xiao** was born in Dongying, Shandong, China. She received her B.E. degree in Polymer Materials and Engineering from Qingdao University of Science and Technology (QUST) and her M.S. degree in Polymer Science from The University of Akron under the supervision of Professor Tianbo Liu. She joined the same research group as a Ph.D. student in 2022. Her research focuses on macroion–counterion interactions, self-assembly, and phase behavior in macroionic systems.

**Bahareh Afsari** is currently pursuing a Ph.D. in Polymer Science and Engineering at the University of Akron. Her research interests focus on polymer physics and supramolecular chemistry, particularly the solution behavior of macroionic systems and chiral interactions, with applications in understanding fundamental physicochemical processes.

**Lake Paul** is the CEO and Founder of BioAnalysis LLC, an agile and collaborative research organization providing quality services and support for gene therapy, biotherapeutics, and the broader life sciences industry. He is an expert in gene therapy analytics, applying biophysical and mass spectrometric methods to protein science. With more than 28 peer-reviewed publications, BLA/MAA submissions, and FDA/EMA responses, Lake frequently speaks at leading scientific conferences around the world.

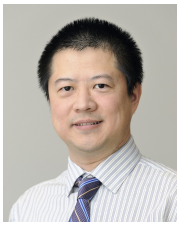

**Tianbo Liu** received his B. S. degree in Chemistry from Peking University, China in 1994 and his Ph.D. in Chemistry from Stony Brook University in 1999 (advisor Benjamin Chu). After spending two more years in the same group as a postdoctoral associate, he started his independent research career at the Physics Department, Brookhaven National Laboratory. In Jan. 2005 he moved to Lehigh University as an assistant professor of Chemistry and was promoted to associate professor in 2009 and full professor in 2012. Since Jan. 2013 he has been the A. Schulman Professor of Polymer Science at The University of Akron. He also served as the Chair of the Department of Polymer Science and the Interim Director of the School of Polymer Science and Polymer Engineering at The University of Akron. His laboratory focuses on understand the fundamental behavior of complex solutions, especially hydrophilic macroions, inorganic-organic hybrid materials and other colloidal and biological systems.